Vol. 86 No. 3 pp. 590–607 ACTA GEOLOGICA SINICA (English Edition) June 2012

Geochemical Characteristics and Metallogenesis of the Qingkuangshan Ni-Cu-PGE Mineralized Mafic-Ultramafic Intrusion in Huili County, Sichuan Province, SW China

ZHU Feilin[1, 2], TAO Yan[1, *], HU Ruizhong[1] and MA Yansheng[3]

1 *State Key Laboratory of Ore Deposit Geochemistry, Institute of Geochemistry, Chinese Academy of Sciences, Guiyang 550002, China*

2 *Graduate University of the Chinese Academy of Sciences, Beijing 100049, China*

3 *East China Geological Exploration Bureau of Nonferrous Metals, Jiangsu Province, Nanjing 210007, China*

Abstract: The Qingkuangshan Ni-Cu-PGE deposit, located in the Xiaoguanhe region of Huili County, Sichuan Province, is one of several Ni-Cu-PGE deposits in the Emeishan Large Igneous Province (ELIP). The ore-bearing intrusion is a mafic-ultramafic body. This paper reports major elements, trace elements and platinum-group elements in different types of rocks and sulfide-mineralized samples in the intrusion. These data are used to evaluate the source mantle characteristics, the degree of mantle partial melting, the composition of parental magma and the ore-forming processes. The results show that Qingkuangshan intrusion is part of the ELIP. The rocks have trace element ratios similar to the coeval Emeishan basalts. The primitive mantle-normalized patterns of Ni-Cu-PGE have positive slopes, and the ratios of Pd/Ir are lower than 22. The PGE compositions of sulfide ores and associated rocks are characterized by Ru depletion. The PGE contents in bulk sulfides are slightly depleted relative to Ni and Cu, which is similar to the Yangliuping Ni-Cu-PGE deposit. The composition of the parental magma for the intrusion is estimated to contain about 14.65 wt% MgO, 48.66 wt% SiO_2 and 15.48 wt% FeOt, and the degree of mantle partial melting is estimated to be about 20%. In comparison with other typical Ni-Cu-PGE deposits in the ELIP, the Qingkuangshan Ni-Cu-PGE deposit has lower PGE contents than the Jinbaoshan PGE deposit, but has higher PGE contents than the Limahe and Baimazhai Ni-Cu deposit, and has similar PGE contents to the Yangliuping Ni-Cu-PGE deposit. The moderate PGE depletions in the bulk sulfide of the Qingkuanghan deposit suggest that the parental magma of the host intrusion may have undergone minor sulfide segregation at depth. The mixing calculations suggests that an average of 10% crustal contamination in the magma, which may have been the main cause of sulfide saturation in the magma. We propose that sulfide segregation from a moderately PGE depleted magma took place prior to magma emplacement at Qingkuangshan, that small amounts of immiscible sulfide droplets and olivine and chromite crystals were suspended in the ascending magma, and that the suspended materials settled down when the magma passed trough the Qingkuangshan conduit. The Qingkuangshan sulfide-bearing intrusion is interpreted to a feeder of Emeishan flood basalts in the region.

Key words: Magmatic sulfide deposit, mafic-ultramafic intrusion, PGE, Qingkuangshan, Emeishan Large Igneous Province

1 Introduction

The Qingkuangshan Ni-Cu-PGE deposit is a sulfide-rich Ni-Cu-PGE deposit. It is located in the Xiaoguanhe region of Huili County, Sichuan Province, where many magmatic sulfide deposits associated with the Emeishan Large Igneous Province (ELIP) occur. There are more than 20 mineralized intrusions in this region, such as the Limahe, Qingkuangshan, Yanghewu, Hetaoshu intrusions (Fig. 1). Based on previous study, these deposits are products of magmatic activity of the ELIP (Yao, 1986; Xu et al., 2001; Zhou et al., 2002; Song et al., 2005, 2006, 2008, 2009;

* Corresponding author. E-mail: taoyan@vip.gyig.ac.cn

Guan et al., 2010).

In the ELIP, magmatic Ni-Cu-PGE deposits associated with mafic-ultramafic intrusions have highly variable sulfide compositions from PGE-rich to PGE-poor (Song et al., 2008), and they can be divided into three types: (1) sulfide-poor PGE deposits, of which the best example is the Jinbaoshan Pt-Pd deposit (Tao et al., 2007a); (2) sulfide-rich Ni-Cu deposit, such as the Baimazhai and Limahe nickel deposits (Tao et al., 2004, 2007b; Wang CY et al., 2005, 2006); (3) sulfide-rich Ni-Cu-PGE deposits such as the Yangliuping and Qingkuangshan Ni-Cu-PGE deposits (Wang et al., 2001; Song et al.,2003, 2008, 2009). The Qingkuangshan Ni-Cu-PGE deposit is same as the Yangliuping Ni-Cu-PGE deposit, which is characterized by enrichments of Cu, Ni and PGE (Song et al., 2008, 2009). All these deposits are related to the ELIP, what caused the variation in sulfide ore compositions? Is it due to the different primary magma or different magma evolution? To answer these questions it is important to understand the relationship between the Cu-Ni-PGE mineralization and the evolution of the ELIP. The Qingkuangshan deposit is a typical Ni-Cu-PGE deposit in the region, it has been poorly studied now, and a further study of the deposit is much needed (Song et al., 2008). This paper reports the results of a integrated study including major elements, trace elements and platinum-group elements in various rock types and mineralized samples from the intrusion. The results are used to evaluate the relationship between the ore-bearing intrusion and the coeval Emeishan flood basalts. And the nature and origin of the primary magma as well as the ore-forming mechanism are discussed. Our results shred new lights on the controls on the formation of magmatic sulfide deposits in the ELIP and are useful for regional mineral exploration.

2 Geological Background

The Qingkuangshan Ni-Cu-PGE deposit is located in the Xiaoguanhe region of Huili County. It is approximately 75 km from Huili City (Fig. 1). The ore-bearing intrusion outcrops in the inner zone of the ELIP where low-Ti basalts are abundant.

Geologically, this deposit is situated in the middle of Kang-Dian massif and is controlled by the Hekou duplex anticline and An-Ning River-Yimen deep fault. In the mining area, there are three groups of faults: SN striking (F_1), NE striking (F_2) and NW striking (F_3). The ore-controlling structure is the SN fault (F_1), which controls the occurrence of the Qingkuangshan intrusion and associated ore body. The NE fault (F_2) and NW fault (F_3) formed later. Due to the effect of NE fault (F_2), the occurrence of SN fault (F_1) was slightly changed: at 1750 level, the fault strikes 10º–20º, dips to SW with the angle of 70º–88º; at 1650 level, the fault strikes south-north, dips to SW with the angle of 64º–71º. Moreover, NW fault (F_3) cutted NE fault (F_2), therefore, the displacement of NE fault (F_2) has happened (Fig. 2).

In the ore district, the main strata are the Middle Proterozoic Hekou Group. The occurrence of the strata is usually NW10º–40º, and the dipping angle is 50º–80º. The main exposed formation is mica schists, with minor lenticular dolomitic marble and carbonaceous slates. From the bottom to top, the strata can be divided into garnet mica schist, mica-schists with quartz-hornstone, mica-schists with dolomitic marble, siliceous slate, quartzite, and black carbonaceous phyllite.

The ore-bearing intrusion intruded the Hekou Group along with south-north fracture. It is an approximately N-S-trending and westward dipping dyke-like body, about 200 m long and 20 to 50 m wide, and the dip angle of this intrusion is almost vertical. The ore-bearing intrusion has a funnel shape in cross section, gradually pinching out downward. The differentiation of the ore-bearing intrusion is significant, especially in the upper parts of intrusion. From the center to both sides, the ore-bearing intrusion is composed of peridotites, olivine pyroxenite (pyroxene peridotite) and gabbro. The ore-bearing intrusion is dominated by peridotites, that makes up about half of all facies.

The ore body is mainly hosted in ultramafic rocks (including peridotite, olivine pyroxenite and pyroxene peridotite), and is concordant with the hosted rocks. It occurs as an approximately N-S-trending len, pinching out in the sides of II and III sections at the surface. It has a tadpole-looking shape in horizontal plane, 150–200 m long with a dipping angle of 60º–88º. It has a funnel shape in cross section, extending for about 150–180m vertically. At depth, the ore body was cut by the NE fault (F_2) to form offset of mineralization. Below the offset fault, the mineralization is mainly uneconomic with economical mineral resource; above the offset fault, the mineralization is mainly economic and forms a funnel-shaped ore body. In different parts of this ore body dipping changes from about 88° in the west to about 50° in the east (Fig. 2). The mineralization is dominated by sparsely disseminated sulfides to densely disseminated sulfides with minor massive sulfide ores (Fig. 3f, g, h). The densely disseminated ores are mainly present in the peridotite at the bottom part of intrusion. With the increasing pyroxene abundance, the grades of the ores decrease. Sparsely disseminated ores often occur above densely disseminated ores; massive ores are mainly controlled by faults and fractures to form saclike bodies. Small massive ores also occur in the central portion of some densely disseminated

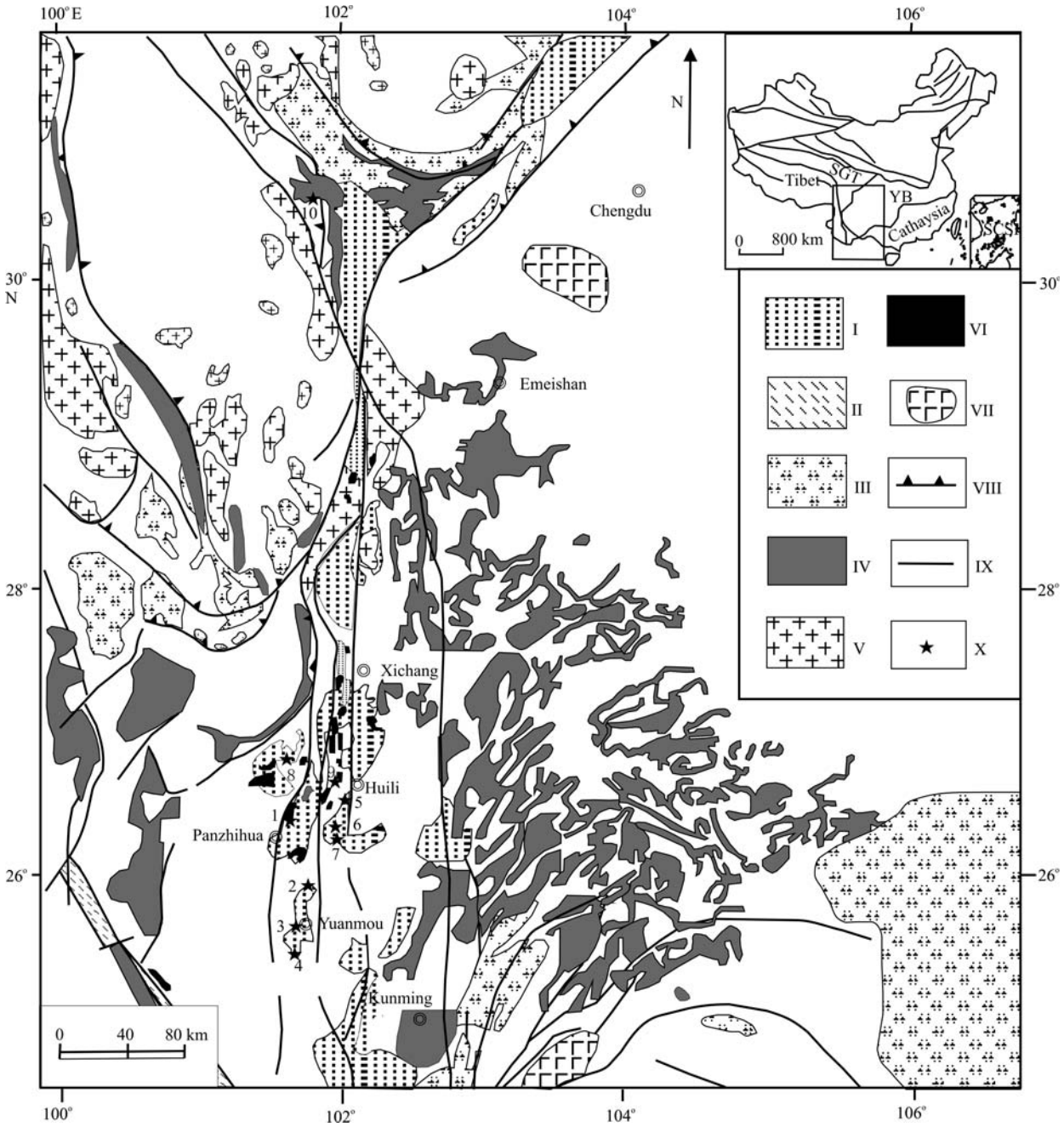

Fig. 1. Regional geological map showing the distributions of the Emeishan Large Igneous Province and associated typical magmatic deposits (modified from Wang et al., 2005).

I, Precambrian Basement; II, Ailaoshan deformed rock; III, Sinian and Palaeozoic rocks; IV, Permian Emeishan flood basalts; V, granite; VI, mafic-ultramafic intrusion; VII, Emeishan basalts found in drill holes; VIII, overthrust fault; IX, fault; X, typical deposit. 1, Panzhihua; 2, Zhubu; 3, Monglingou; 4, Anyi; 5, Limahe; 6, Hetaoshu; 7, Qingkuangshan; 8, Dacao; 9, Hongge; 10, Yangliuping.

ores (The original 401 Geological Brigade of Sichuan Bureau of Geology and Mineral Resources，1960[1]; Yao, 1986).

3 Petrographic Characteristics

Samples were collected from tunnel, including all kinds of rocks and ores. The rocks are made up of ultramafic rocks and mafic rocks including olivine pyroxenite, pyroxene peridotite, plagioclase-bearing pyroxene peridotite, pyroxenite and gabbro; and the ores include sparsely disseminated ore, densely disseminated ore and minor massive ore (Fig. 3f, g, h).

The ore-bearing olivine pyroxenite and pyroxene peridotite have the character of dull black medium-fine grained texture as well as massive texture. The major rock-forming minerals in these rocks are basically the same, but the abundances of olivine and pyroxene in olivine

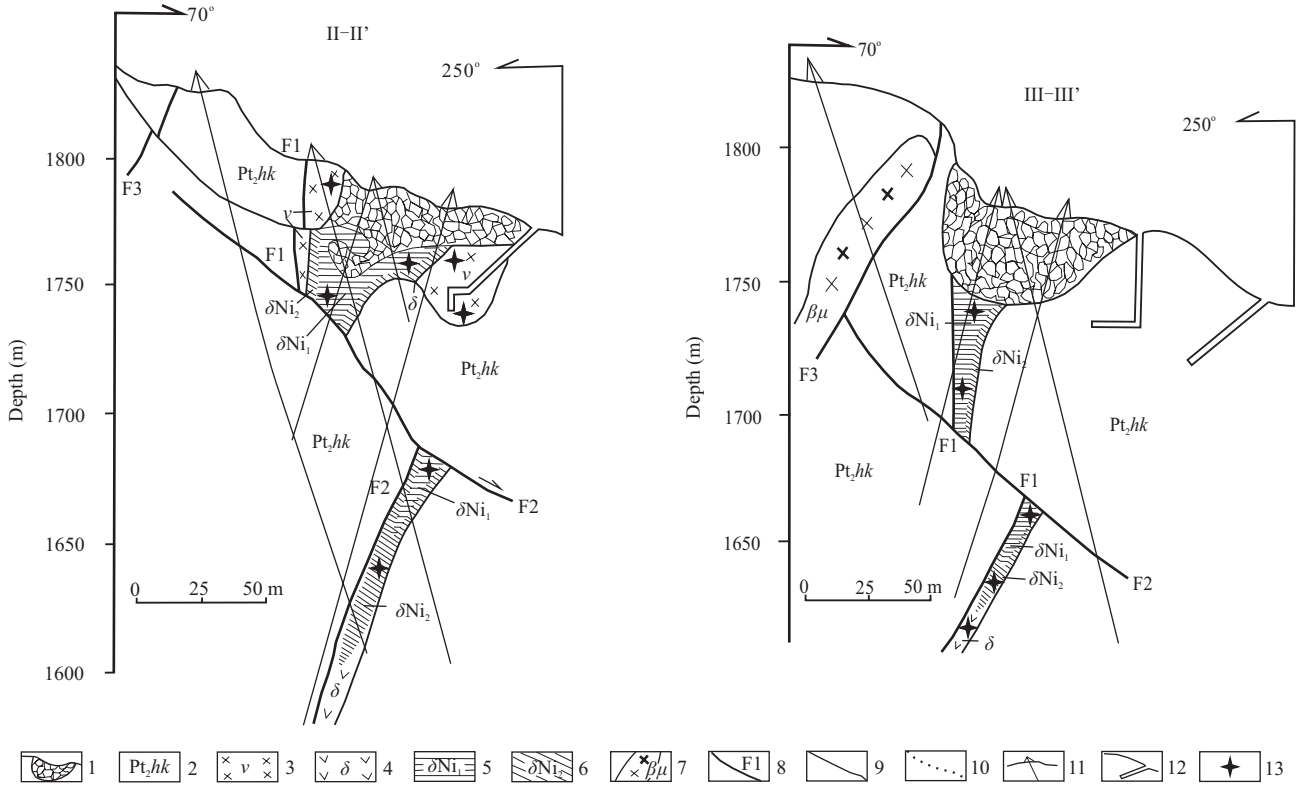

Fig. 2. The cross-section of the Qingkuangshan Ni-Cu-PGE deposit (modified from Yao, 1986).
1, Goaf; 2, metamorphic rock series of the Hekou Group; 3, gabbro; 4, peridotite; 5, economical mineral resource of peridotite; 6, uneconomical mineral resource of peridotite; 7, diabase; 8, fault and its number; 9, geological boundary; 10, transitional geological boundary; 11, drill hole; 12, tunnel; 13, sampling position.

pyroxenite and pyroxene peridotite are different, the major rock-forming minerals that mainly consist of olivine (about 20%–60%) and pyroxene (about 70%–30%) with minor plagioclase (about 2%–3%); and the abundance of plagioclase in the plagioclase-bearing pyroxene peridotite is slightly higher (about 5%). The grain sizes of olivine are highly variable. They have been partially serpentinized but peritectic texture is still preserved (Fig. 3a). Pyroxenes are dominated by clinopyroxene plus minor orthopyroxene. Plagioclases has a labradorite composition. It commonly exhibits tabular twins (Fig. 3b). In the ultramafic rocks, metallic minerals are dominanted by pyrrhotite, pentlandite and chalcopyrite. Minor pyrite, chromite and magnetite are also present. They occur as disseminated assemblages, as small veins in the fractures of silicates and rarely as larger sulfide patches (Fig. 3c, d). Because of different crystallization temperatures different minerals crystallized at different times. Based on textural observations the metallic minerals are inferred to have crystallized in the following order: chromite, pyrrhotite, pentlandite, magnetite, pyrite and chalcopyrite.

Pyroxenites have the character of dull black, coarse to fine grained texture, as well as massive texture. Pyroxene crystals are euhedral or subhedral. In pyroxenites, the contents of pyroxene can reach up to 80% plus minor olivine, amphibole and plagioclase. The rocks are mostly not sulfide- mineralized or contain rare sulfides.

Gabbros have the character of dark grey to grey, medium to fine grained texture, as well as massive texture. Pyroxene crystals are subhedral to xenomorphic. Sulfides are rare commonly. The main rock forming minerals are pyroxene (about 50%) and plagioclase (about 30%) with minor biotite (about 5%) and amphibole, accessory minerals are apatite, ilmenite, titanite and so on.

4 Samples and Analytical Methods

The compositions of major rock-forming minerals were analyzed using an EPMA-1600 electron mincroprobe in the State Key Laboratory of Ore Deposit Geochemistry, Institute of Geochemistry, Chinese Academy of Sciences, Guiyang, China. The diameter of electron-beamt, accelerating voltage and beam current were 22 um, 25 kV, 10 nA, respectively. The sulfide-bearing rocks and sulfide-barren rocks were analyzed for major, trace and rare earth element compositions. The samples analyzed include olivine pyroxenite, pyroxene peridotite, plagioclase-bearing pyroxene peridotite, pyroxenite and gabbro. The analyses of major elements, trace elements and rare earth elements were done by the ALS Chemex. The samples for

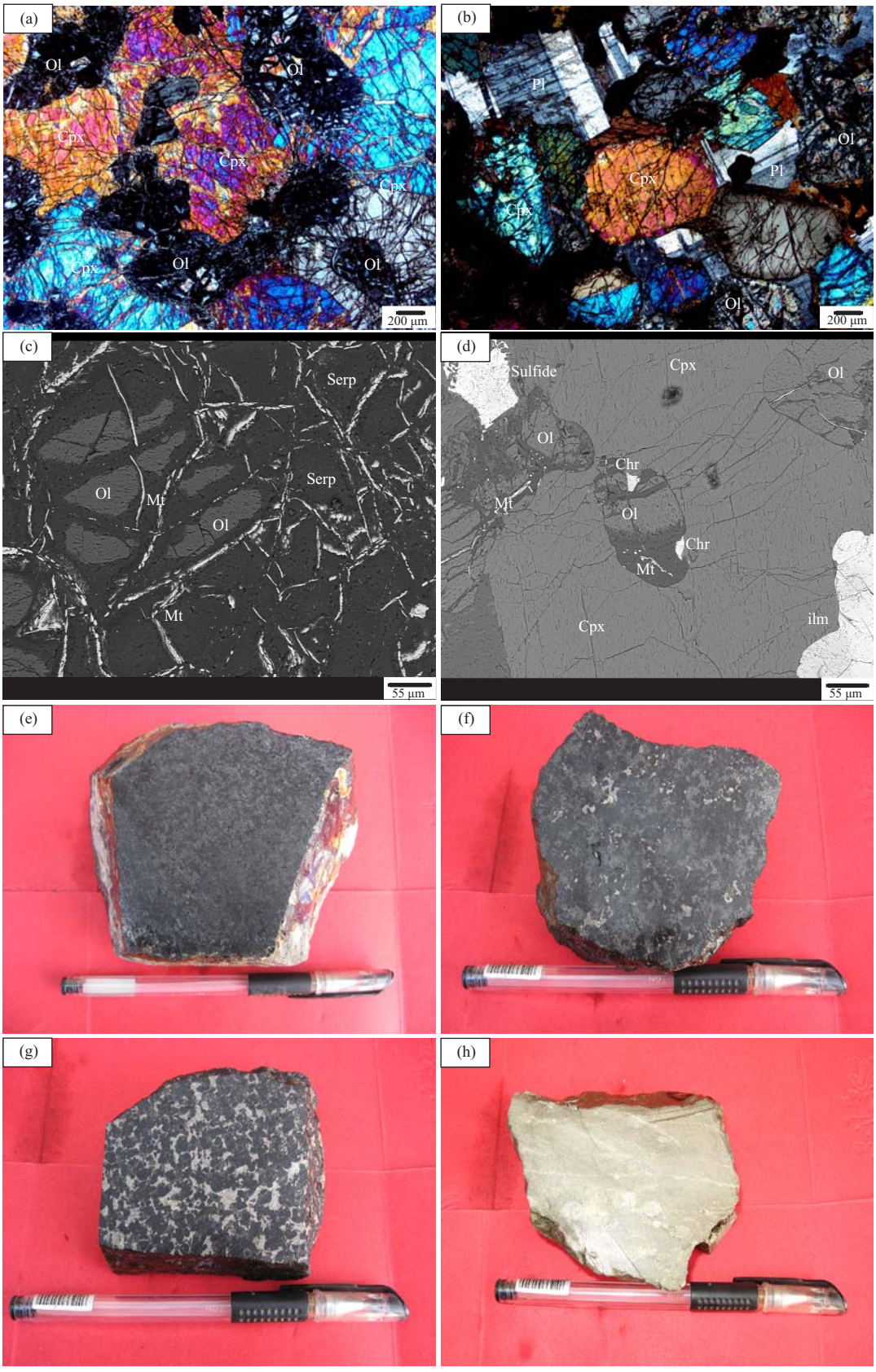

Fig. 3. Back-scattered electron images and microphotographs of some samples in Qingkuangshan Ore-bearing rocks and the photographs of main types of ore

a, Olivine (Ol) enclosed within clinopyroxene (Cpx) and has the crystal stack structure; b, between the olivine and the clinoenstenite distributes the few plagioclase feldspar which has double crystal phenomenon; c, magnetite (MT) occurs as micro-scale veinlets along the crack of olivine; d, few big pellet chromite(Chr); e, olivine websterite; f, sparsely disseminated ore; g, densely disseminated ore; h, massive ore.

major elements analysis were prepared using lithium metaborate or lithium tetraborate menstruum and analyzed by ICP-AES. The detection limits are about 0.01 wt%. The samples for trace and rare earth element analysis were prepared using lithium metaborate and analyzed by ICP-MS. The concentrations of PGEs in the samples were determined in the National Research Centre for Geoanalysis in Beijing by ICP-MS. The analytical procedures of PGEs are the same as in Zhang et al. (2005b), and detection limits are Os 0.007 ppb, Ir 0.013 ppb, Ru 0.02 ppb, Rh 0.001 ppb, Pt 0.026 ppb and Pd 0.06 ppb.

5 Geochemical Characteristics

5.1 Mineral chemistry

Table 1 lists the representative compositions for major rock-forming minerals in the ultramafic rocks. Generally, the olivines have a great change in the particles size (about 0.2–0.5 mm) and are enclosed in pyroxenes, most of them are fresh, and only small fractions have the serpentinized phenomena. Olivine has a chrysolite composition (Fo=78–85). Pyroxenes crystals in the ultramafic rocks are mainly diopside with minor bronzite, and the bronzite generally grow in diopside.

The nickel content in olivine of the Qingkuangshan intrusion is 1000–1500 ppm (Table 1). The nickel content of the parental magma is estimated to be 100–150 ppm. Olivine crystals of the Qingkuangshan intrusion exhibit a positive Ni-Fo correlation, which suggest that they formed by fractional crystallization of a single parental magma. Modeling shows that 9%–10% fractional crystallization of picritic magma can explain the observed olivine compositions (Fig. 4). In comparison with olivine from the Jinbaoshan Pt-Pd deposit (nickel content 1500–2000 ppm), the nickel contents of olivine from the Qingkuangshan intrusion is lower, which may be due to early sulfide segregation in the parental magma of the Qingkuangshan intrusion.

5.2 Major elements

The analytical results of the major elements in whole rocks are listed in Table 2. The SiO_2 and MgO contents of mafic-ultramafic rocks are between 33.5 wt%–49.9 wt% and 7.13 wt%–27.2 wt% respectively. The CaO/Al_2O_3 varies between 0.88 and 4.40. Generally, the mafic-ultramafic rocks are high in MgO but low in Al_2O_3, P_2O_5, K_2O and Na_2O. The m/f ratios of these rocks are between 0.66 and 4.92, within the range for ferric mafic-ultramafic rocks. Due to variable hydrothermal alteration and sulphide contents, the LOI values are highly variable.

The Harker diagrams (Fig. 5) show that, due to variable post-magmatic hydrothermal alteration, as the contents of MgO decrease, the contents of Al_2O_3, K_2O, Na_2O and TiO_2 in the samples increase. SiO_2 contents increase with decreasing MgO content but then decreased. The P_2O_5 and FeOt contents show no clear trends. Generally, the compositional variations in the Qingkuangshan mafic-ultramafic rocks are similar to that of the coeval Emeishan picrites.

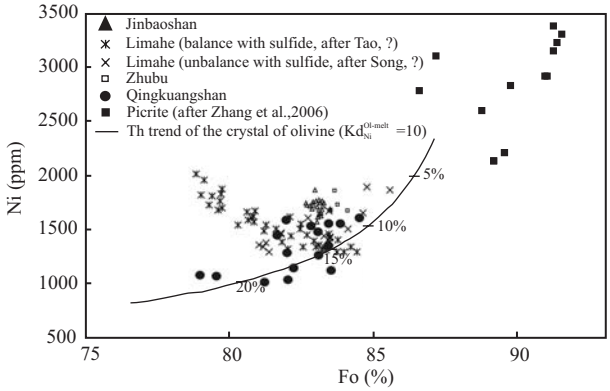

Fig. 4. Plots of Fo versus Ni contents for olivine in the ultramafic rocks of the Qingkuangshan intrusion.
Picrites from Zhang et al., 2006; Jinbaoshan from Tao et al., 2007a; Zhubu from Tao (unpublished data); curve on the figures represent the number of olivine crystals.

5.3 The characteristics of rare earth and trace element compositions

The concentrations and ratios of REE and trace elements are listed in Table 3.

5.3.1 Rare earth elements

The total REE contents of the mafic-ultramafic rocks are rather low as compared to the Emeishan picrites (except the high contents of QK0818 and QK0821), as a whole, the mafic rocks have higher total REE contents than the ultramafic rocks of the intrusion. The mafic-ultramafic rocks have 1.59–2.79 $(La/Sm)_N$, 7.85–12.19 $(La/Yb)_N$, 6.80–11.21 $(Ce/Yb)_N$, 5.93–8.99 $(\Sigma\omega(Ce)/\Sigma\omega(Y))$. The chondrite-normalized REE patterns of the mafic-ultramafic rocks are similar to that of OIB such as LREE enrichments relative to HREE. However the contents of REE in the Qingkuangshan mafic-ultramafic rocks are lower than those in OIB (Fig. 6a). Overall, the mafic-ultramafic rocks are characterized by normal to negative anomalies of δCe and δEu values ranging from 0.92 to 1.04 and from 0.89 to 1.12, respectively. The Eu negative anomalies may have been in part due to plagioclase fractional crystallization or post-magmatic hydrothermal alteration (Zhong et al., 2004). Alternatively contamination with crustal material may have also caused the Eu negative anomalies.

Table 1 Representative analyses of rock-forming minerals in the ultramafic rocks from the Qingkuangshan magmatic Ni-Cu-PGE sulfide deposit (oxides: wt% and Ni: ppm)

Mineral	No.	Point No.	SiO_2	Al_2O_3	MgO	FeO	CaO	Na_2O	K_2O	TiO_2	Cr_2O_3	MnO	NiO	P_2O_5	Total	Ni	Fo
olivine	QK1	1	39.82	0.01	42.09	16.77	0.24	0.00	0.00	0.01	0.03	0.23	0.16	0.00	99.37	1273	81.9
	QK1	3	41.12	0.12	43.43	15.33	0.22	0.01	0.00	0.02	0.08	0.18	0.20	0.03	100.74	1603	83.6
	QK1	4	40.90	0.01	42.84	15.92	0.27	0.00	0.00	0.03	0.06	0.23	0.20	0.00	100.46	1572	82.9
	QK1	5	39.68	0.01	39.05	19.53	0.38	0.00	0.00	0.03	0.07	0.24	0.13	0.15	99.28	1029	78.3
	QK1	7	39.72	0.04	42.40	16.58	0.31	0.01	0.01	0.04	0.05	0.25	0.14	0.02	99.56	1116	82.2
	QK1	9	39.28	0.00	40.89	17.32	0.22	0.00	0.01	0.04	0.08	0.23	0.12	0.05	98.24	959	81.0
	QK1	10	40.95	0.00	43.65	15.41	0.12	0.02	0.01	0.03	0.39	0.21	0.17	0.00	100.96	1352	83.6
	QR4	10	41.11	0.01	42.33	14.83	0.64	0.00	0.00	0.00	0.10	0.22	0.14	0.04	99.42	1084	83.7
	QR4	11	39.88	0.02	43.62	14.86	0.24	0.00	0.01	0.04	0.23	0.19	0.20	0.05	99.33	1603	84.1
	QR7	1	39.45	0.00	39.82	20.19	0.26	0.00	0.01	0.05	0.05	0.27	0.09	0.12	100.31	731	78.0
	QR7	4	39.61	0.00	44.09	14.13	0.28	0.01	0.01	0.02	0.11	0.18	0.21	0.00	98.66	1674	84.9
	QR7	7	40.04	0.01	39.74	18.42	0.29	0.01	0.01	0.04	0.17	0.23	0.08	0.07	99.11	660	79.5
	QR7	9	39.79	0.01	42.10	16.73	0.30	0.00	0.00	0.01	0.08	0.23	0.12	0.01	99.38	974	81.9
clino-pyroxene	QK1	12	52.05	3.44	14.81	5.77	22.19	0.24	0.00	1.17	0.94	0.12	0.02	0.07	100.80		
	QK1	13	52.00	3.12	15.10	5.54	21.41	0.28	0.00	1.20	0.79	0.08	0.03	0.07	99.62		
	QR4	4	52.54	1.70	15.90	5.20	21.63	0.16	0.02	0.82	0.57	0.13	0.03	0.04	98.73		
	QR4	17	52.29	2.46	15.71	6.07	21.02	0.23	0.01	1.03	0.54	0.13	0.02	0.07	99.56		
	QR4	20	51.82	2.50	15.35	5.47	21.66	0.26	0.00	0.99	0.58	0.12	0.04	0.05	98.84		
	QR6	3	53.42	2.45	15.74	4.87	22.20	0.24	0.00	0.78	0.97	0.10	0.02	0.03	100.80		
	QR6	4	54.26	1.61	16.26	4.51	20.95	0.22	0.01	0.67	0.75	0.11	0.00	0.00	99.36		
	QR6	14	53.15	2.40	15.86	4.49	21.47	0.23	0.00	0.85	1.10	0.10	0.03	0.01	99.69		
	QR7	8	48.98	5.35	13.28	6.87	21.82	0.35	0.00	2.17	0.42	0.12	0.01	0.02	99.37		
	QR7	11	50.88	3.17	15.00	5.21	21.16	0.29	0.01	1.03	1.10	0.10	0.02	0.04	98.03		
	QR7	12	52.00	2.98	15.32	5.17	21.63	0.18	0.00	1.12	1.05	0.11	0.00	0.04	99.60		
	QR7	13	46.80	6.94	12.38	7.34	21.29	0.41	0.02	2.84	0.37	0.14	0.00	0.03	98.55		
ortho-pyroxene	QR4	18	53.61	2.73	25.79	14.35	1.57	0.02	0.00	0.39	0.06	0.29	0.00	0.07	98.88		

Table 2 Major oxide and sulfur contents of the Qingkuangshan mafic-ultramafic rocks (wt%)

object	gabbro	pyroxenite	pyroxene peridotite		pyroxenite		gabbro	pyroxene peridotite		olivine websterite			plagioclase-bearing pyroxene peridotite	gabbro
No.	QK0807	QK0810	QK0812	QK0814	QK0815	QK0817	QK0818	QK0819	QK0821	QK1	QK2	QK5	QR1	QR7
SiO_2	44.60	37.80	33.50	40.00	49.90	48.40	49.50	47.50	43.10	37.00	38.80	38.60	38.60	43.60
TiO_2	0.68	0.69	1.04	0.54	0.89	1.16	3.37	0.96	1.21	1.49	1.06	0.52	0.51	1.77
Al_2O_3	2.31	2.26	3.36	1.88	2.92	4.86	6.75	3.48	7.71	2.85	3.45	1.7	1.96	6.16
Fe_2O_3	14.3	18.7	21	17.05	7.46	12.6	12.5	11.95	21.4	18.4	16.15	15.4	12.95	13.55
MnO	0.11	0.12	0.16	0.13	0.12	0.14	0.20	0.11	0.12	0.21	0.17	0.15	0.16	0.16
MgO	20.90	23.70	18.30	24.20	18.70	14.80	9.98	15.35	7.13	23.00	23.20	26.90	27.20	18.50
CaO	9.03	2.58	5.52	5.08	12.85	12.9	10.15	14.5	6.77	7.29	9.23	7.00	6.49	8.48
Na_2O	0.24	0.20	0.32	0.27	0.32	0.63	2.20	0.34	1.83	0.35	0.43	0.18	0.21	0.78
K_2O	0.08	0.12	0.27	0.11	0.09	0.47	0.54	0.20	0.81	0.11	0.17	0.05	0.11	0.37
Cr_2O_3	0.96	0.56	0.27	0.47	0.44	0.31	0.11	0.40	0.06	0.46	0.49	0.55	0.24	0.85
P_2O_5	0.01	0.03	0.12	0.13	0.03	0.08	0.13	0.06	0.02	0.06	0.06	0.03	0.05	0.11
LOI	6.46	11.30	8.83	8.34	4.11	3.53	3.24	5.31	7.35	6.85	6.81	8.94	11.75	4.32
Total	99.68	98.06	92.69	98.2	97.83	99.88	98.67	100.20	97.51	98.1	100.00	100.00	98.80	98.80
S	2.17	3.89	5.9	2.49	0.54	1.72	0.27	2.81	5.08	2.54	2.03	1.97		
$Mg^{\#}$	74.51	71.71	63.54	73.95	83.37	70.14	61.49	71.98	39.99	71.43	74.18	77.75	80.77	73.19
m/f	2.90	2.52	1.73	2.81	4.92	2.32	1.57	2.54	0.66	2.47	2.84	3.46	4.14	2.69

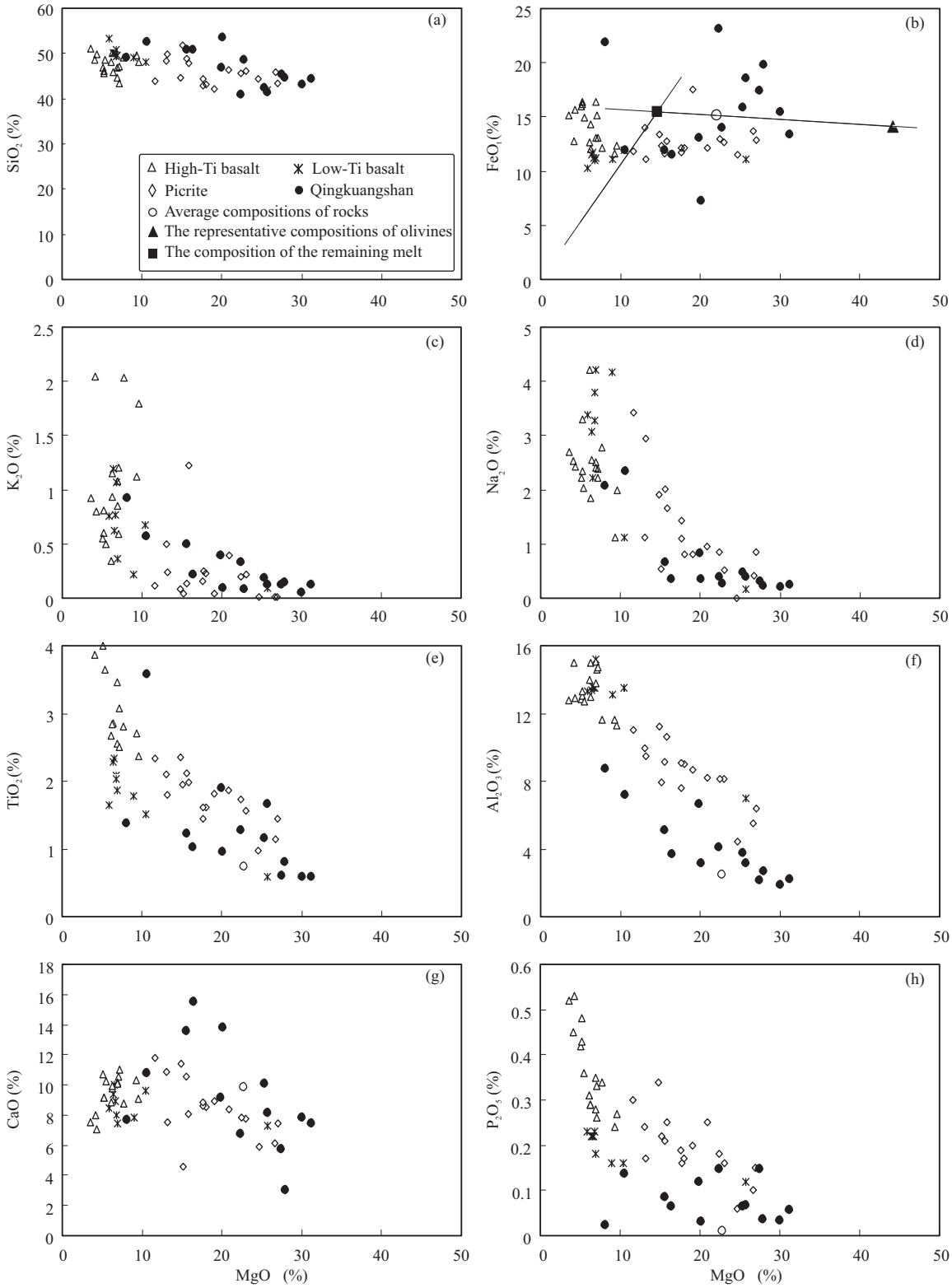

Fig. 5. Diagram of MgO versus major oxides of the Qingkuangshan intrusion.
Picrites from Zhang et al., 2006; high Ti basalts and low Ti basalts from Xu et al., 2001.

5.3.2 Trace elements

The primitive mantle-normalized trace element patterns of the mafic-ultramafic rocks are similar to that of OIB except for slight depletion of Ba, Nb, Ta, Sr and Ti, and enrichments of Th and U (Fig. 6b). The depletions of Nb, Ta, Ti and Zr may have been due to crustal assimilation which is present in the coeval basalts (Xu et al., 2001; Xiao et al., 2004; Zhang et al., 2006; Tao et al., 2007b). The

Table 3 Trace element concentrations (ppm) and eigenvalues of the Qingkuangshan mafic-ultramafic rocks.

object	gabbro	pyroxenite	pyroxene peridotite		pyroxenite		gabbro	pyroxene peridotite		olivine websterite			plagioclase-bearing pyroxene peridotite	gabbro
No.	QK0807	QK0810	QK0812	QK0814	QK0815	QK0817	QK0818	QK0819	QK0821	QK1	QK2	QK5	QR1	QR7
Sc	12	12	16	9	12	10	6	11	6	8	7	7		
V	47	65	94	39	56	75	86	54	105	115	102	19	38	103
Cr	6510	3780	1600	2940	3140	2190	780	2880	430	3160	3500	3940	1600	6060
Co	183	298	417	233	98.4	157	130.5	172.5	448	225	213	237	131.5	114
Ni	2300	5710	12100	3940	1140	2850	136	3480	12200	3710	2420	3050		
Cu	4050	9850	8490	7280	2220	5250	234	6880	12000	5340	3630	4420		
Rb	3.3	5.6	14.2	5.2	3.6	21	28.1	9.2	41.7	3.8	5.3	2	5.1	11.7
Sr	75.7	42.9	92.2	50.3	93.6	117	146	80.2	144	75.7	101	43.1	66.6	220
Y	4.9	4.6	7.4	3.8	6.4	11.1	17.8	8.5	19	5.8	7.3	3.6	3.7	10.7
Zr	35	44	63	32	43	72	184	53	128	51	62	26	35	105
Nb	3.5	5.1	7.4	4.1	4.5	9.6	33.4	6.2	13.4	6.2	6.4	2.7	4	14.1
Ba	24.4	37	119	29.1	24.8	102.5	164.5	38.8	224	38.2	49.9	17.4	32.9	138.5
La	4.2	5.6	8	4.1	5.3	11.9	23.7	7	21.2	5.8	7.4	3.3	5.1	13.7
Ce	10	12.2	18.3	9.3	12.9	27.3	56.9	17.1	44.7	13	17.1	7.1	10	31.6
Pr	1.48	1.67	2.53	1.31	1.93	3.73	7.61	2.46	5.77	1.91	2.46	1.09	1.39	4.38
Nd	6.6	7.1	10.8	5.7	8.9	15.7	30.7	11.2	23.7	8.8	11.5	5.1	6.1	19.2
Sm	1.6	1.58	2.37	1.24	2.15	3.43	6.08	2.64	4.9	1.95	2.66	1.2	1.27	3.99
Eu	0.47	0.48	0.78	0.38	0.59	0.94	1.4	0.77	0.93	0.66	0.85	0.4	0.43	1.4
Gd	1.5	1.43	2.19	1.12	1.86	3.07	5.39	2.48	4.37	1.98	2.6	1.17	1.18	3.66
Tb	0.2	0.22	0.32	0.17	0.28	0.46	0.76	0.36	0.64	0.28	0.36	0.16	0.18	0.51
Dy	1.1	1.04	1.61	0.83	1.42	2.3	3.6	1.84	3.49	1.45	1.85	0.86	0.86	2.64
Ho	0.19	0.18	0.29	0.15	0.25	0.43	0.65	0.35	0.65	0.24	0.32	0.15	0.16	0.46
Er	0.52	0.48	0.75	0.37	0.65	1.15	1.82	0.85	1.8	0.65	0.84	0.36	0.39	1.17
Tm	0.05	0.05	0.08	0.04	0.07	0.14	0.22	0.1	0.21	0.08	0.1	0.04	0.04	0.14
Yb	0.36	0.36	0.51	0.28	0.46	0.9	1.41	0.64	1.65	0.48	0.59	0.29	0.3	0.86
Lu	0.05	0.05	0.07	0.04	0.06	0.13	0.21	0.09	0.2	0.06	0.08	0.04	0.04	0.12
Hf	1.1	1.2	1.8	0.8	1.3	2.1	5.5	1.6	3.3	1.5	1.9	0.8	1	2.9
Ta	0.2	0.4	0.5	0.3	0.3	0.6	2.6	0.4	0.8	0.4	0.4	0.2	0.3	0.9
Th	0.37	0.58	0.81	0.42	0.48	2.36	7.18	0.72	6.89	0.62	0.87	0.32	0.53	1.47
U	0.11	0.17	0.26	0.13	0.14	0.79	1.59	0.22	1.18	0.17	0.24	0.09	0.15	0.38
Ti	1100	1600	2100	1000	1500	1300	2900	1100	2000	1800	1500	700		
ΣREE (without Y)	28.32	32.44	48.6	25.03	36.82	71.58	140.45	47.88	114.21	37.34	48.71	21.26	27.44	83.83
Σω(Ce)/ Σω(Y)	6.13	7.51	7.35	7.34	6.29	7.34	8.99	6.14	7.78	6.15	6.23	5.93	7.71	7.77
δEu	0.93	0.98	1.05	0.99	0.90	0.89	0.75	0.92	0.61	1.03	0.99	1.03	1.07	1.12
δCe	0.98	0.98	1.00	0.98	0.99	1.00	1.04	1.01	0.99	0.96	0.98	0.92	0.92	1.00
$(La/Yb)_N$	8.37	11.16	11.25	10.50	8.26	9.48	12.06	7.85	9.22	8.67	9.00	8.16	12.19	11.43
$(La/Lu)_N$	9.00	12.00	12.25	10.99	9.47	9.81	12.10	8.34	11.36	10.36	9.91	8.84	13.66	12.24
$(La/Sm)_N$	1.69	2.29	2.18	2.13	1.59	2.24	2.52	1.71	2.79	1.92	1.80	1.78	2.59	2.22
$(Ce/Yb)_N$	7.72	9.41	9.97	9.23	7.79	8.43	11.21	7.42	7.53	7.52	8.05	6.80	9.26	10.21
$(Gd/Lu)_N$	3.71	3.53	3.87	3.46	3.83	2.92	3.17	3.41	2.70	4.08	4.02	3.62	3.65	3.77
Nb/Zr	0.10	0.12	0.12	0.13	0.10	0.13	0.18	0.12	0.10	0.12	0.10	0.10	0.11	0.13
Zr/Y	7.14	9.57	8.51	8.42	6.72	6.49	10.34	6.24	6.74	8.79	8.49	7.22	9.46	9.81
Zr/Nb	10.00	8.63	8.51	7.80	9.56	7.50	5.51	8.55	9.55	8.23	9.69	9.63	8.75	7.45
Ta/Yb	0.56	1.11	0.98	1.07	0.65	0.67	1.84	0.63	0.48	0.83	0.68	0.69	1.00	1.05
Th/Yb	1.03	1.61	1.59	1.50	1.04	2.62	5.09	1.13	4.18	1.29	1.47	1.10	1.77	1.71
Gd/Yb	4.17	3.97	4.29	4.00	4.04	3.41	3.82	3.88	2.65	4.13	4.41	4.03	3.93	4.26
La/Nb	1.20	1.10	1.08	1.00	1.18	1.24	0.71	1.13	1.58	0.94	1.16	1.22	1.28	0.97
Th/Nb	0.11	0.11	0.11	0.10	0.11	0.25	0.21	0.12	0.51	0.10	0.14	0.12	0.13	0.10

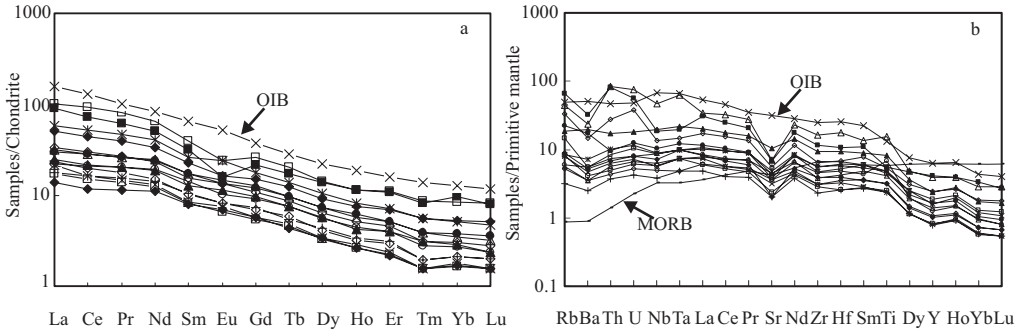

Fig. 6. Chondrite-normalized REE patterns and primitive mantle-normalized trace element patterns for the Qingkuangshan mafic-ultramafic rocks.
CI, OIB, MORB and Primitive mantle values after Sun and MacDonough, 1989.

subparallel primitive mantle-normalized trace element patterns of the mafic-ultramafic rocks suggest that these rocks are related to a single magma.

5.4 Ni, Cu, and platinum-group elements

The concentrations of PGE, Cu and Ni in whole rock samples are listed in Table 4. The primitive mantle-normalized Ni-PGE-Cu patterns of the sulfide-bearing samples in recalculated 100% sulfide and sulfide-barren samples are illustrated in Fig. 7. These plots show that all samples from the Qingkuangshan intrusion are enriched in PPGE (Pt, Pd) relative to IPGE (Os, Ir, Ru and Rh), Ru depletion is present in the samples.

Previous studies have showed that the primitive mantle-normalized PGE patterns of mantle xenoliths, Alps-type peridotites and komatiites are nearly flat and have lower Pd/Ir ratios. The enrichments of PPGE relative to IPGE in Qingkuangshan samples may have been related to mantle partial melting, furthermore, variation in mantle source compositions and mantle partial melting can also contribute to the fractionation of PGE in mantle-derived magma (Tao et al., 2004). The Qingkuangshan intrusion is thought to have derived from magma generated in an OIB-type mantle characterized by PPGE enrichments and high Pd/Ir ratios ranging from 10 to 30. In the plot of Ni/Cu-Pd/Ir (Fig. 8), the Qingkuangshan samples mainly fall within the field of high-Mg basalt or below it, suggesting that the primary magma of the Qingkuangshan intrusion formed by high degree of mantle partial melting.

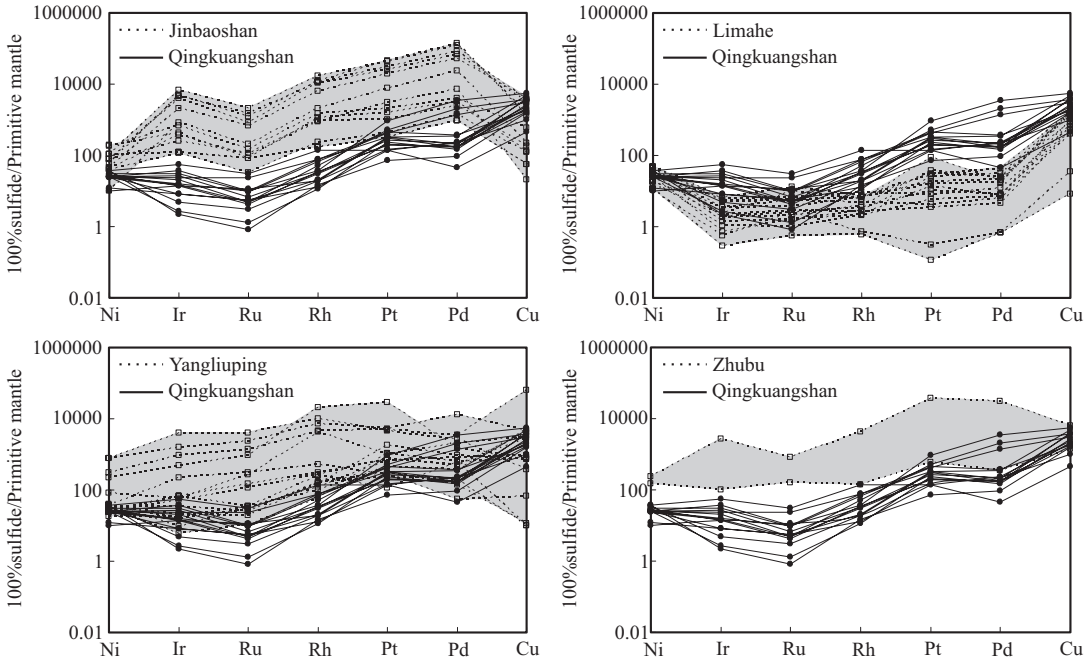

Fig. 7. Primitive mantle-normalized Ni-PGE-Cu patterns of sulfide ores on a 100% sulfide basis and sulfide-barren rocks of the Qingkuangshan Ni-Cu-PGE magmatic sulfide deposit.
Cu, Ni, PGE of primitive mantle values after Barnes and Maier, 1999; Jinbaoshan and Limahe from Tao et al., 2007a, 2008; Zhubu from Zhu et al., 2007; Yangliuping from Song et al., 2003, 2008.

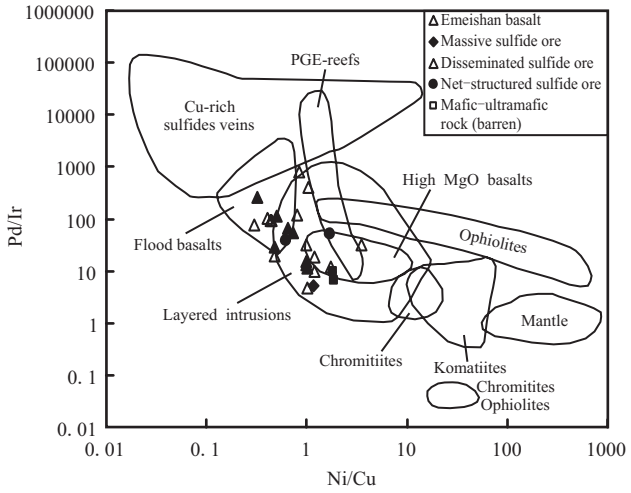

Fig. 8. Ni/Cu against Pd/Ir ratios diagram for the Qingkuangshan intrusion (Fields from Barnes and Lightfood, 2005; Emeishan basalts from Zhong et al., 2006).

6 Discussion

6.1 Parental magma compositions

Previous studies showed that the ratios of chalcophile elements (Ni, Cu and PGE) are rarely affected by crustal contamination and mainly reflect the composition of parental magma (e.g., Keays, 1995). Ultramafic magmas usually give rise to Ni-dominated sulfide deposits with Ni/Cu ratios higher than 7, such as the komatiite-associated Ni deposits in Kambalda, Western Australia (Ni/Cu=13.5) (Lesher et al., 1984). Mafic magmas commonly produce Ni-Cu-(PGE) sulfide deposits with Ni/Cu usually less than 2 (Naldrett, 2004), such as the Noril'sk Ni-Cu-PGE deposits, Siberia (Ni/Cu=0.5–1.06) and the Voisey's Bay Ni-Cu-Co deposit, Canada (Ni/Cu=1.87). As shown in Table 4, the Qingkuangshan samples have an average Ni/Cu ratio of 1.03, with a small range of 0.48 to 1.85. Therefore, the Qingkuangshan intrusion may have derived from a mafic magma.

Under equilibrium conditions, olivine composition reflects the composition of the magma from which the olivine crystallized. Thus, using Mg-Fe exchange coefficient (K_d= $[(FeO/MgO)_{Ol}/(FeO/MgO)_{magma}]_{molar}$=0.3–0.34) (Roder and Emslie, 1970; Hanson and Langmuir, 1978; Ulmer, 1989; Thompson and Gibson, 2000) and the composition of most Mg-rich olivine in the rocks (Chai and Naldrett, 1992), we can estimate the parental magma composition. The most Mg-rich olivine in the Qingkuangshan intrusion is Fo=84.9, which corresponds to an MgO/(MgO+FeO) value of 0.946 for the liquid in equilibrium with olivine, based on a distribution coefficient of K_d=0.3(Roeder and Emslie, 1970). We then estimated other oxide contents in the magma based on of the correlation between MgO and other oxides (Fig. 5b). The average estimated values are 14.65% MgO, 48.66% SiO_2, 15.48% FeOt, 0.93% Na_2O, 0.42% K_2O and 1.80% TiO_2.

If values for the most Mg-rich olivine compositions from a sample plot on an olivine–liquid equilibrium curve at approximately the same FeO content as present in the bulk rock, the MgO content of the rock is close to that of the liquid from which the olivine crystallized. The calculated MgO/(MgO+FeO) value is much lower than the MgO/(MgO+FeO) values of the Qingkuangshan intrusive rocks. In Fig. 9 olivine Mg-number is plotted vs. whole-rock MgO content, the compositions of the most Mg-rich olivine plot below the liquid-olivine mixing line of closed system, indicating excess (cumulus) olivine in the samples (Zhang and Wang, 2003; Chai et al., 2007). Due to re-equilibration with trapped silicate liquid before complete solidification, final olivine is less Mg-rich than original cumulus crystals. Therefore, the estimated MgO content for the parental magma is likely less than the true value (Wu et al., 2004).

In terms of the major elemental discrimination of Hawaiian picrites in primary magma (MgO=16%–21%) (Hirschmann and Ghiorso, 1994; Norman and Garcia, 1999; Herzberg and O'Hara, 2002), the estimated parental magma for Qingkuangshan area is low-Ti tholeiite with the character of high-Mg (Fodor, 1990; Xu et al., 2001), far from high-Ti basalt with the character of low-Mg from ELIP (Xiong et al., 1984).

Figure 10 compares the Qingkuangshan intrusion with associated volcanic rocks using incompatible trace elements such as La, Sm, Gd, Yb and Y, and their ratios such as La/Sm, Gd/Yb, and Ti_2O/Y. Samples from the Qingkuangshan intrusion, low-Ti basalts and picrites of the ELIP have similar trends, which are significantly different from coeval high-Ti basalts. The results show that the parental magmas of the Qingkuangshan mafic-ultramafic intrusion are similar to of the coeval low-Ti basalts reported previously by Xiao et al. (2004), suggesting that the Qingkuangshan mafic-ultramafic intrusion was produced

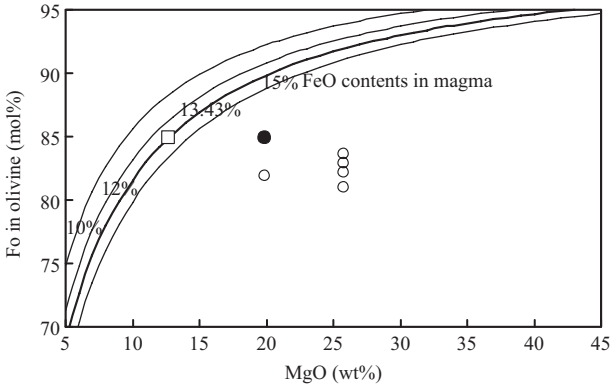

Fig. 9. Diagram of MgO-Fo-FeO.
●, the highest Fo values of olivine; ○, the other high Fo values of olivine; □, primitive magma.

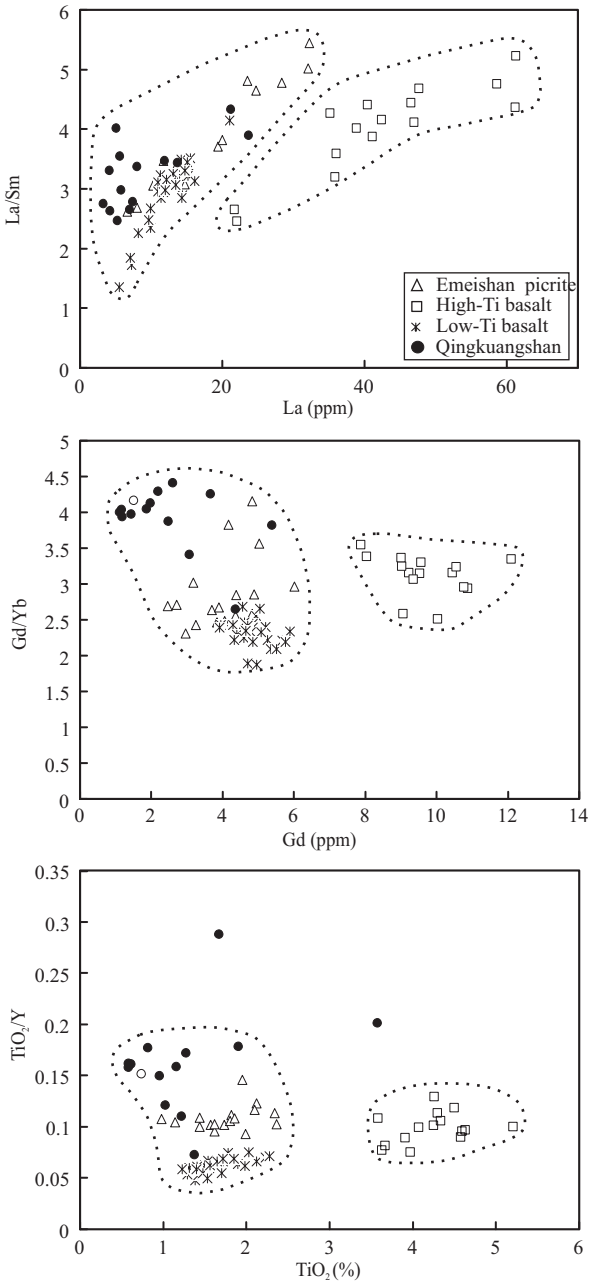

Fig. 10. Plots of trace elements on La/Sm-La, Gd/Yb-Gd and TiO_2/Y-TiO_2 (Picrites from Zhang et al., 2006; high Ti basalts and low Ti basalts from Xiao et al., 2004)

by higher degree of mantle partial melting.

6.2 Petrogenesis

Because Yb is compatible in garnet but not in clinopyroxene, Sm/Yb ratio can be used to constrain mantle source mineralogy of alkaline magmas (Aldanmaz et al., 2000). Fig. 11 is the plot of garnet-dependent Sm/Yb ratio vs. Sm. It can be seen that the Qingkuangshan mafic-ultramafic rocks have high Sm/Yb ratios, consistent with the products of magma derived from a mantle garnet-lherzolite. This is supported by high $(Gd/Yb)_{pm}$ ratios (2.2–3.6) of the samples. Magma derived from a garnet-stable source mantle is expected to have high $(Gd/Yb)_{pm}$ ratios because the garnet-melt partition coefficients for HREE are much higher than those for LREE.

On the basis of some correlatively researches for source characters of ELIP in recent years (e.g. Xu et al., 2004; Zhang et al., 2005a; Zhou et al., 2006; Xu et al., 2007), and the aforementioned discussion of source characters for Qingkuangshan intrusion, the magmatic source of Qingkuangshan intrusion was being analogous to oceanic island basalts sources. And based on this condition, using the content of REE in primary magma, we can estimate the degree of mantle partial melting by way of that:

$F=C_i^{source}/C_i^{magma}$,

F—the degree of partial melting of the mantle,

i—the strong incompatible element i,

C_i^{source}—the content of strong incompatible element in source region,

C_i^{magma}—the content of strong incompatible element in primary magma,

The approach to estimate the content of strong incompatible elements in primary magma (e.g. REE) is to use the method of the Li. (1986)❷

$REE_i^{melt}=REE_i^{rock}/(1-f+K_i^{Ol\text{-}melt}\times f)$,

i—the rare earth element (REE),

REE_i^{melt}—the content of REE in primary magma，

REE_i^{rock}—the content of REE in rocks,

$K_i^{Ol\text{-}melt}$—the distribution coefficient of REE between olivine and melt (after Bedard, 1999),

f—the weight percentage of olivine in their coexistence melt (f=0.415). The method of estimating the weight percentage of olivine is the principle of mass balance. We absorb the way of Tao et al. (2002) to estimate the weight percentage of olivine in their coexistence melt.

The estimated results of the degree of partial melting for the primary magma of the Qingkuangshan intrusion are

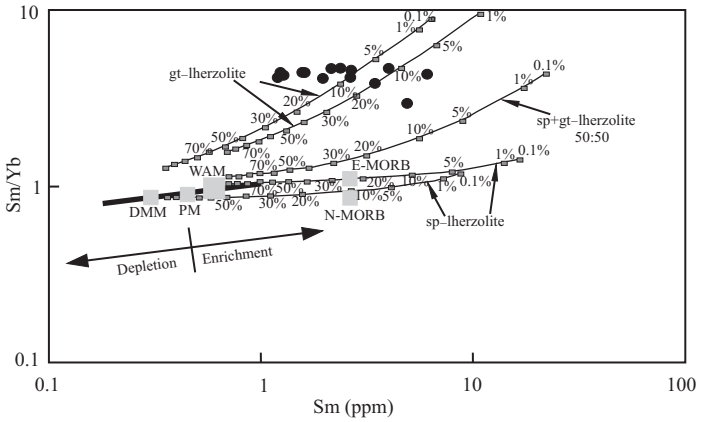

Fig. 11. Plot of Sm-Sm/Yb showing melt curves for Qingkuangshan intrusion (after Aldanmaz et al., 2000).

listed in Table 5. According to the contents of La and Ce elements in Qingkuangshan mafic-ultramafic intrusion, the corresponding degrees of partial melting for the primary magma are respective 23.8% and 22.6%. Considering the influences of crustal assimilation, the calculated value is high than the true value, it is roughly estimated that about 20%. That high degree of partial melting for the primary magma corresponding to lower Pd/Ir ratio (about 22) (Chu et al., 2001).

6.3 Crustal contamination

$(Nb/Th)_{pm}$ is best used to indicate the extent of Nb anomaly and $(Th/Yb)_{pm}$ is a sensitive indicator of crustal contamination, so, the degree of crustal contamination of the magmas can be estimated using $(Nb/Th)_{pm}$ and $(Th/Yb)_{pm}$ ratios where the rock values have been normalized to the relevant trace element content of the primitive mantle (Zhou et al., 2008; Wang, 2008).

In Fig. 12, the $(Nb/Th)_{pm}$ vs $(Th/Yb)_{pm}$ diagram, we assume that these mafic-ultramafic rocks are formed from a mixture of different proportions of mantle-derived magma and crustal contaminant. For the mantle-derived end member, we used two compositions, one being N-MORB (Sun and McDonough, 1989) and the other being the most primitive and least contaminated picrites of the west Emeishan flood basalt province. For the crustal end member, owing to lack of systematic analytical data of the upper crust sediments for this region, we used the average compositions of the upper crust and lower crust (Taylor and Mclennan, 1985). Compared to N-MORB, the Qingkuangshan rocks have lower $(Nb/Th)_{pm}$ but higher $(Th/Yb)_{pm}$ ratios, consistent with a high degree of crustal contamination. And compared to the upper crust and lower crust or the lithosphere (Taylor and Mclennan, 1985), the contents of Th element have a large range of variation from 0.4 ppm to 7.0 ppm which have some similarities with the former. The results of the comparison showed that the Qingkuangshan intrusion has underwent the contamination by little lithospheric or crustal before the formation of the rocks. The simulation results show that, using N-MORB as the mantle-derived end member do not correspond with the evolutionary trend of Qingkuangshan rocks, whereas the use of the average composition of the Emeishan picrites as the mantle-derived gives a good fit, and the degree of crustal contamination of the Qingkuangshan rocks varied from 3% to 12% by the upper crust.

6.4 Sulfur saturation and sulfide segregation

Keays pointed out whether the magmas had reached sulfide saturation was the crucial factor for the formation of the sulfide magmatic deposit. Experimental and theoretical studies suggest that Pd can be strongly concentrated in

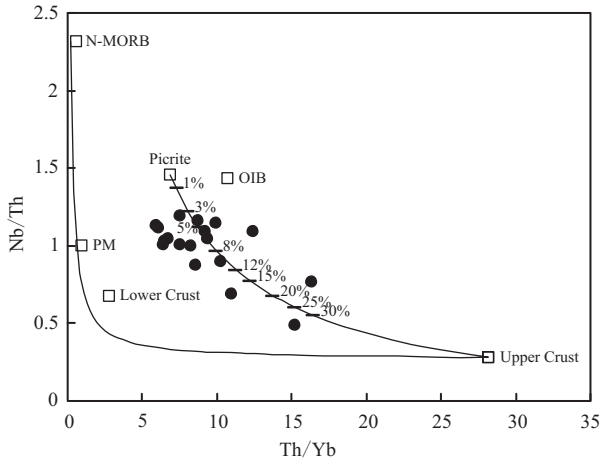

Fig. 12 $(Th/Yb)_{pm}$ vs $(Nb/Th)_{pm}$ diagram showing the degrees of crustal contamination.
Primitive mantle, OIB and MORB after Sun and MacDonough (1989); upper and lower crust after Taylor, S.R and Mclennan, S.M (1985); picrites from Zhang et al., 2006; curve on the figures represent the degrees of crustal contamination; partial data from mining companies'material.

sulfide, owing to the much larger sulfide liquid-silicate liquid partition coefficient for Pd (17000) relative to Cu (~1383), therefore, Cu/Pd ratio is an effective tool to evaluate sulfide saturation in magmas (Barnes and Maier, 1999). If the magma was S-unsaturated, Cu and Pd behave as incompatible elements, and therefore the Cu/Pd ratios of a primary magma should be similar to those observed for the mantle (about 6300) (Barnes et al., 1988); but in sulfide unsaturated magma, the Cu/Pd ratios of a primary magma should be much greater than 6300.

Almost all the samples from Qingkuangshan intrusion are characterized by Cu/Pd ratios higher than 6300, this may be due to the fact that sources of these basalts retained residual sulfides during melting or sulfide saturation had occurred in the early stage of magma evolution. The above discussion has shown that, because of the relatively large degree of partial melting of the mantle and the phenomenon of moderate PGE depletion in ores, the high Cu/Pd ratios for almost all the samples are unlikely due to retention of sulfides in the mantle. Therefore, the above analysis and evidence indicate that, during the magma ascent, the parental magmas had reached sulfide saturation and caused sulfide segregation, and then led to the formation of weakly PGE depleted magma.

From the Pd-Cu/Pd diagram (Fig. 13), we can see that different types of Ni-Cu-PGE magmatic sulfide deposit in Emeishan Large Igneous Province have different distribution. The Limahe and Baimazhai Ni-Cu deposits are characterized by strong depletion in PGE relative to Ni and Cu, with lower Pd and high Cu/Pd ratios（greater than 200000); the Jinbaoshan Pt-Pd deposit is characterized by the enrichment of PGE, with higher Pd and low Cu/Pd

Table 4 Copper, nickel (ppm) and PGE (ppb) concentrations and eigenvalues for the sulfide ores and sulfide-barren rocks of the Qingkuangshan magmatic Ni-Cu-PGE sulfide deposit

object	sparsely disseminated ore			olivine websterite	gabbro	sparsely disseminated ore		densely disseminated ore		massive ore
No.	QK1	QK2	QK5	QR1	QR7	QK09-T2	QK09-T9-1	QK09-K8	QK09-K12	QK09-T9-2
Ni	3420	2550	2970	1070	637	1160	6790	8960	24900	49600
Ir	8.45	2.65	2.48	1.96	0.75	0.64	1.22	2.21	2.39	122.96
Ru	3.27	1.27	1.14	0.70	0.75	0.65	0.88	1.98	1.35	101.14
Rh	4.78	1.54	1.72	0.68	0.32	0.45	1.46	2.34	4.52	86.56
Pt	215.00	75.40	72.40	40.80	25.80	52.25	233.80	276.81	167.50	621.08
Pd	96.30	35.50	37.60	18.90	4.94	18.68	79.40	86.58	121.10	626.52
Cu	3370	2590	3000	585	344	2440	10550	14600	14700	42200
Cu/Pd	34995	72958	79787	30952	69636	130623	132875	168628	121391	67356
Pd/Ir	11.40	13.40	15.16	9.64	6.59	29.14	64.91	39.18	50.64	5.10
Pd/Pt	0.45	0.47	0.52	0.46	0.19	0.36	0.34	0.31	0.72	1.01
Pt/Pd	2.23	2.12	1.93	2.16	5.22	2.80	2.94	3.20	1.38	0.99
Ni/Cu	1.01	0.98	0.99	1.83	1.85	0.48	0.64	0.61	1.69	1.18

Table 5 Estimating the degree of partial melting for the primary magma of the Qingkuangshan intrusion (REE: ppm)

		La	Ce	Pr	Nd	Sm	Eu	Gd	Tb	Dy	Ho	Er	Tm	Yb	Lu
The distribution coefficient① (olivin/melt)		0.0003	0.0003	0.0003	0.0002	0.00018	0.0002	0.00025	0.000475	0.0007	0.00122	0.00174	0.00384	0.00522	0.00852
Primary magma (Inversion result)	1	7.18	17.09	2.53	11.28	2.73	0.80	2.56	0.34	1.88	0.32	0.89	0.09	0.61	0.08
	2	9.57	20.85	2.85	12.14	2.70	0.82	2.44	0.38	1.78	0.31	0.82	0.09	0.61	0.08
	3	13.67	31.28	4.32	18.46	4.05	1.33	3.74	0.55	2.75	0.50	1.28	0.14	0.87	0.12
	4	7.01	15.89	2.24	9.74	2.12	0.65	1.91	0.29	1.42	0.26	0.63	0.07	0.48	0.07
	5	9.06	22.05	3.30	15.21	3.67	1.01	3.18	0.48	2.43	0.43	1.11	0.12	0.78	0.10
	6	20.34	46.66	6.37	26.83	5.86	1.61	5.25	0.79	3.93	0.73	1.96	0.24	1.53	0.22
	7	40.50	97.24	13.01	52.47	10.39	2.39	9.21	1.30	6.15	1.11	3.11	0.38	2.40	0.36
	8	11.96	29.22	4.20	19.14	4.51	1.32	4.24	0.62	3.14	0.60	1.45	0.17	1.09	0.15
	9	36.23	76.39	9.86	40.51	8.37	1.59	7.47	1.09	5.96	1.11	3.07	0.36	2.81	0.34
	10	9.91	22.22	3.26	15.04	3.33	1.13	3.38	0.48	2.48	0.41	1.11	0.14	0.82	0.10
	11	12.65	29.22	4.20	19.66	4.55	1.45	4.44	0.62	3.16	0.55	1.43	0.17	1.00	0.14
	12	5.64	12.13	1.86	8.72	2.05	0.68	2.00	0.27	1.47	0.26	0.61	0.07	0.49	0.07
	13	17.60	38.45	5.20	22.05	4.51	1.45	4.15	0.56	2.75	0.50	1.31	0.15	0.94	0.14
	14	8.72	17.09	2.38	10.43	2.17	0.73	2.02	0.31	1.47	0.27	0.67	0.07	0.51	0.07
	15	23.41	54.01	7.49	32.82	6.82	2.39	6.26	0.87	4.51	0.79	2.00	0.24	1.46	0.20
	avg	15.56	35.32	4.87	20.97	4.52	1.29	4.15	0.60	3.02	0.54	1.43	0.16	1.09	0.15
Mantle sources		3.70	8.00	0.97	3.85	1.00	0.30	0.76	0.11	0.56	0.11	0.26	0.04	0.22	0.03
The degree of partial melting (%)		23.8	22.6	19.9	18.4	22.1	23.2	18.3	18.5	18.6	20.3	18.2	24.3	20.1	20.1

Note: ①-after Bedard JH, 1999; ②-after Arndt and Christensen,1992.

ratios (lower than 1000); and the Yangliuping and Zhubu deposits are characterized by intermediate Pd contents and Cu/Pd ratios. Song et al. (2008) pointed out that Yangliuping deposit was produced by extensive sulfide segregation from weakly PGE-depleted magmas, because of earlier sulfide removal. Samples from the Qingkuangshan, Yangliuping and Zhubu deposits have similar trends, which show that Qingkuangshan deposit was produced by extensive sulfide segregation from weakly PGE-depleted magmas.

In order to study the influence of sulfide segregation on Qingkuangshan intrusion, it is necessary to do the model calculation via the following equation of Campbell and Naldrett (1979): $C_i^{Sul}=C_i^{Sil}\times D_i^{Sul/Sil}\times(R+1)/(R+D_i^{Sul/Sil})$, where C_i^{Sul} and C_i^{Sil} represent the concentrations of element i in the sulfide melt and in the parental silicate magma, respectively; $D_i^{Sul/Sil}$ is the sulfide melt/silicate liquid partition coefficient of element i; and R is the R-factor.

On the basis of the aforementioned discussion of magmatic origin for Qingkuangshan intrusion, we assume that the ELIP basaltic magmas had 15 ppb Pt, 22 ppb Pd, 1 ppb Ir, and 200 ppm Cu before reaching S-saturation, which represents the primary magma of the Qingkuangshan intrusion. The model calculation result (Fig. 13) indicates that the parental magma had undergone a small amount of segregation sulfide lost (about 0.014%) in the early magma evolution, which led to the formation of moderately PGE depleted magma. Subsequently, the moderately PGE depleted magma underwent the further contamination and further sulfide segregation with R-factors ranging from 1000 to 6000, and then led to the formation of sulfide melts, which are roughly consistent with the contents of Pd, Ni and Cu of the pure sulfide melts of the Qingkuangshan PGE ores.

6.5 A diagenetic and metallogenic model

Studies showed that PGE contents in primary magma are strongly dependent on the composition of mantle-derived rocks, the degree and the mechanism of mantle partial melting. Keays (1995), Rehkämper et al. (1999) and Peach (1996) assume that the primitive mantle had 4 ppb Pd and 250 ppm S, if the degree of batch partial melting was about 20%, the content of Pd in melts can reach to the theoretically maximum value (about 20 ppb). So far, the search has not been reported of the content of Pd in primary magma more than 40 ppb. Hamlyn et al. (1985) had reported that the Boninites derived from the depleted mantle have very high content of Pd with the highest

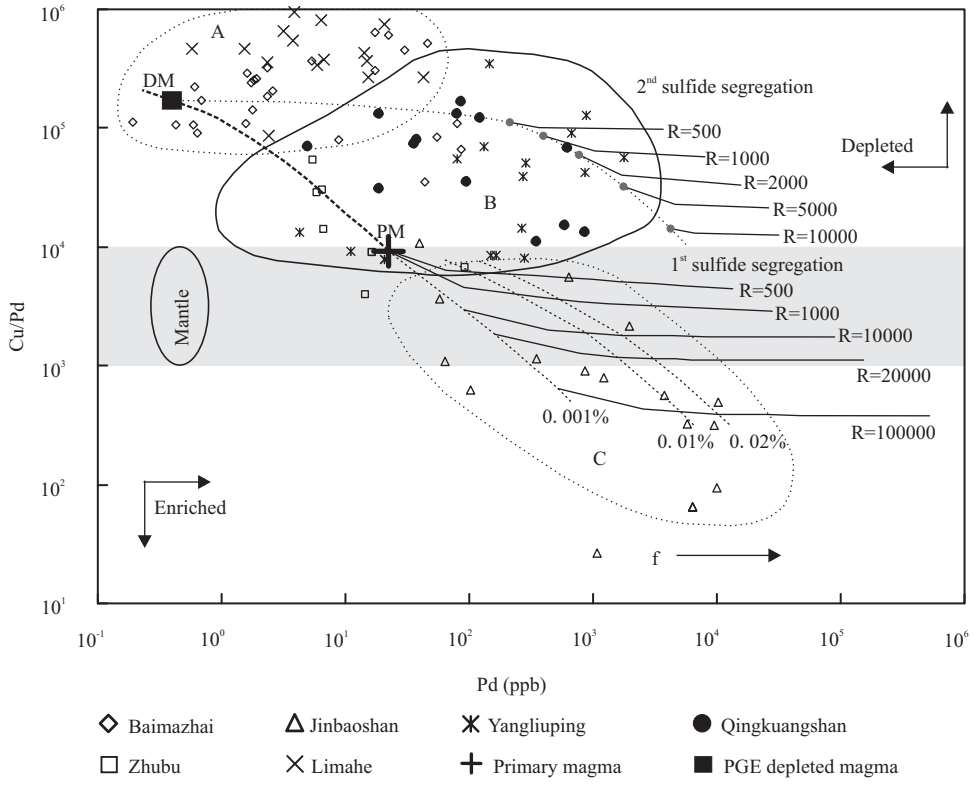

Fig. 13. Pd vs Cu/Pd diagram of typical Ni-Cu-PGE magmatic sulfide deposits in Emeishan Large Igneous Province.

F, content of segregated sulfide; A, the distribution of Limahe and Baimazhai; B, the distribution of Yangliuping and Zhubu; C, the distribution of Jinbaoshan. Primitive mantle values after Sun and MacDonough, 1989; Limahe from Tao et al., 2008; Baimazhai from Wang CY et al., 2006; Zhubu from Zhu et al., 2007; Yangliuping from Song et al., 2008; Jinbaoshan from Tao et al., 2007a.

content of Pd (about 38 ppb), but the content of Pd in the melts derived from undepleted mantle is generally less than 30 ppb. The content of Pd in Qingkuangshan ore-bearing intrusion is far higher than 30 ppb with the average content of 100 ppb, which is well above the highest content of Pd in the melts derived from any mantle by partial melting, indicating that the primary magma of Qingkuangshan intrusion had undergone the accumulation of PGE before the formation of Qingkuangshan deposit.

The concentration of cumulate segregated sulfides in magma can trigger the accumulation of Cu, Ni and PGE; therefore, sulfide segregation is the main controlling factors on metallogenesis of magmatic sulphide deposit. The Qingkuangshan deposit is marked by relatively high PGE grades was thought to have been formed by accumulation of immiscible sulfide droplets from a large amount of magma in a sill-like conduit.

According to the calculation of sulfide segregation shown in Fig. 13, in the early stage of magma evolution, about 0.014% sulfide melt removal from the PGE rich primary magma would give rise to a moderately PGE depleted magma. Subsequently, owing to the contamination by crustal materials for moderately PGE depleted magma (ranging from 3% to 12%), the sulfides segregated from the moderately PGE depleted magma under R values ranging from 1000 to 6000, and mixed with olivine and chromite in the staging chamber to form mineral-laden mush. In a word, the intrusion was formed by concentration of cumulate minerals and segregated sulfides in magma conduit system.

7 Conclusions

(1) The major and trace elements variations of the Qingkuangshan mafic-ultramafic rocks show that the Qingkuangshan mafic-ultramafic rocks are products of magmatic activity in the ELIP, and their evolutionary trend is corresponding with Emeishan picrites; by estimating, the primary magma is picritic, with degree of about 20% mantle partial melting which is analogous to the source mantle of OIB;

(2) The segregation model analysis indicates that the ore-forming magma had undergone a small amount of segregation sulfide lost (about 0.014%) in the early magma evolution, which led to the formation of moderately PGE depleted magma, subsequently, the moderately PGE depleted magma underwent the further contamination and further strong sulfide segregation, and then led to the formation of sulfide ores with the character of moderate PGE-depletion;

(3) The model calculation suggests that the ore sulfides segregated from the moderately PGE depleted magma and mixed with olivine and chromite in the staging chamber to form mineral-laden mush, subsequently, the intrusion was formed by concentration of cumulate minerals and segregated sulfdes in magma conduit system.

Acknowledgements

The authors thank the two anonymous reviewers for their help in improving the quality of the manuscript. We are also very grateful to the National Research Center, the senior engineer of Zheng Wenqin and Dr Liu Shirong (Institute of Geochemistry, Chinese Academy of Sciences) for their kind help with the lab work. This study was financially supported by the Chinese Academy of Sciences (grant no. KZCX2-YW-Q04-06), the National Key Basic Research Program of China (grant no. 2009CB421005), and the National Science Foundation of China (grant no. 40973039).

Manuscript received Apr. 8, 2011
accepted July 27, 2011
edited by Fei Hongcai

Note

❶ The original 401 Geological Brigade of Sichuan Bureau of Geology and Mineral Resources. 1960. Field investigation.

❷ Li Changnian. 1986. Trace elements and their using in petrology, staff room of Wuhan Geology College (internal communication.

References

Arndt, N.T., and Christensen, U., 1992. The role of lithospheric mantle in continental flood volcanism: Themal and geochemical constraints. *J. Geophys. Res*, 97: 10967–10981.

Aldanmaz, E., Pearce, J.A., Thirlwall, M.F., and Mitchell, J.G., 2000. Petrogenetic evolution of late Cenozoic, post-collision volcanism in western Anatolia, Turkey. *Journal of Volcanology and Geothermal Research*, 102: 67–95.

Barnes, S.J., Boyd, R., Korneliussen, A., Nilsson, L.P., Often, M., Pedersen, R.B., and Robins, B., 1988. The use of mantle normalization and metal ratios in discriminating between the effects of partial melting, crystal fractionation and sulfide segregation on platinum-group elements, gold, nickel and copper: examples from Norway. In: Prichard, H.M., Potts, P.J, Bowles, J.F.W., and Cribb, S.J. (eds), *Geo-Platinum 87.* Symp Vol., London: Elsevier Applied Science, 113–143.

Barnes, S.J., and Maier, W.D., 1999. The fractionation of Ni, Cu and the noble metals in silicate and sulphide liquids. In: Keays, R.R., Lesher, C.M., Lightfood, P.C., and Farrow, C.E. (eds), *Dynamic Processes in Magmatic Ore Deposits and Their Application to Mineral Exploration*. Geological Association of Canada Short Course Notes, 13: 69–106.

Barnes, S.J., and Lightfood, P.C., 2005. Formation of magmatic nickel sulfide ore deposits and processes affecting their copper and platinum group element contents. *Economic Geology*, 100: 179–213.

Bedard, J.H., 1999. Petrogenesis of boninites from the Betts Cove Ophiolite, Newfoundland, Canada: Identification of

subducted source components. *Journal of Petrology*, 40(12): 1853–1889.

Campbell, I.H., and Naldrett, A.J., 1979. The influence of silicate: sulfide ratios on the geochemistry of magmatic sulfides. *Economic Geology*, 74(6): 1503–1506.

Chai Fengmei, Zhang Zhaochong, Dong Lianhui, Zhang Zuoheng, Wu Hua and Li Jun, 2007. Geochemistry and petrogenesis of the Baishiquan Cu-Ni sulfide-bearing mafic-ultramafic intrusion in the Central Tianshan, Xinjiang, NW China. *Acta Petrologica Sinica*, 23(10): 2366–2378 (in Chinese with English abstract).

Chai Gang and Naldrett, A.J., 1992. The Jinchuan ultramafic intrusion: Cumulate of a high-Mg basaltic magma. *J. Petrology*, 33(2): 227–303.

Chu Xuelei, Sun Min and Zhou Meifu, 2001. The platinum-group element geochemistry in chemical geodynamics. *Acta Petrologica Sinica*, 17(1): 112–122 (in Chinese with English abstract).

Fodor, R.V., Sial, A.N., and Mukasa, S.B., 1990. Petrology , isotopic characteristics and K-Ar ages of the Maranhao, Northern Brazil, Mesozoic basalt province. *Comtr. Miner. Petrol*, 104: 555–567.

Guan Jianxiang and Song Xieyan, 2010. Platinum-group elements as ore potentiality tracers of a few small mafic-ultramafic intrusions in Panxi area, Sichuan Province. *Mineral Deposits*, 29(2): 207–217 (in Chinese with English abstract).

Hamlyn, P.R., Keays, R.R., Cameron, W.E., Crawford, A.J., and Waldron, H.M., 1985. Precious metals in magnesian low-Ti lavas: implications for metallogenesis and sulfur saturation in primary magmas. *Geochimica et Cosmochimica Acta*, 49: 1797–1811.

Hanson, G.N., and Langmuir, C.H., 1978. Modelling of major elements in mantle-melt systems using trace element approaches. *Geochimica et Cosmochimica Acta*, 42: 725–741.

Herzberg, C., and O'Hara, M.J., 2002. Plume-associated ultramafic magmas of Phanerozoic age. *Journal of Petrology*, 43: 1857–1883.

Hirschmann, M.M., and Ghiorso, M.S., 1994. Activities of nickel, cobalt, and manganese silicates in magmatic liquids and appli-cations to olivine/liquid and to silicate/melt partitioning. *Geochimica et Cosmochimica Acta*, 58: 4109–4126.

Keays, R.R., 1995. The role of komatiitic and picritic magmatism and S-saturation in the formation of ore deposits. *Lithos,* 34: 1–18.

Lesher, C.M., Arndt, N.T., and Groves, D.I., 1984. Genesis of komatiite-associated nickel sulfide deposits at Kambalda, Western Australia: a distal volcanic model. In: Buchanan, D.L., and Jone, M.J. (eds), *Sulfide deposits in mafic and ultramafic rocks*. Institute of Mining Metallurgy, London, 70–80.

Naldrett, A.J., 2004. *Magmatic sulfide deposit: geology, geochemistry and exploration*. Springer, Berlin Heidelberg New York, 137–277.

Norman, M.D., and Garcia, M.O., 1999. Primitive magmas and source characteristics of the Hawaiian plume: Petrology and geochemistry of shield picrites. *Earth and Planetary Science Letters*, 168: 27–44.

Peach, C.L., and Mathez, E.A., 1996. Constraints on the formation of platinum-group element deposits in igneous rocks. *Economic Geology*, 91: 439–450.

Rehkämper, M., Halliday, A.N., Fitton, J.G., Lee, D.C., Wieneke, M., and Arndt, N.T., 1999. Ir, Ru, Pt, and Pd in basalts and komatiites:New constraints for the geochemical behavior of the platinum-group elements in the mantle. *Geochimica et Cosmochimica Acta*, 63: 3915–3934.

Roeder, P.L., and Emslie, R.F., 1970. Olivine-liquid equilibrium. *Contrb. Mineral. Petrol*., 29: 275–289.

Song Xieyan, Zhou Meifu, Cao Zhimin, Sun Min and Wang Yunliang, 2003. Ni-Cu-(PGE)magmatic sulfide deposits in the Yangliuping area, Permian Emeishan igneous province, SW China. *Mineralium Deposita*, 38: 831–843.

Song Xieyan, Zhang Chengjiang, Hu Ruizhong, Zhong Hong, Zhou Meifu, Ma Runze and Li Youguo, 2005. Genetic links of magmatic deposits in the Emeishan Large igneous Province with dynamics of mantle plume. *Jounal of Minerology and Petrology*, 25(4): 35–44 (in Chinese with English abstract).

Song Xieyan, Zhou Meifu, Keays, R.R., Cao Zhimin, Sun Min and Qi Liang, 2006. Geochemistry of the Emeishan flood basalts at Yangliuping, Sichuan, SW China: implications for sulfide segregation. *Contrib. Mineral. Petrol*., 152: 53–74.

Song Xieyan, Zhou Meifu, Tao Yan and Xiao Jiafei, 2008. Controls on the metal compositions of magmatic sulfide deposits in the Emeishan large igneous province, SW China. *Chemical Geology*, 253: 38–49.

Song Xieyan, Hu Ruizhong and Chen Liemeng, 2009. Geochemical natures of copper, nickel and PGE and their significance for the study of origin and evolution of mantle-derived magmas and magmatic sulfide deposits. *Earth Science Frontiers*, 16(4): 287–305 (in Chinese with English abstract).

Sun, S.S., and McDonough, W.F., 1989. Chemical and isotopic systematics in ocean basalt: Implication for mantle composition and processes. In: Saunders, A.D., and Norry, M.J. (eds), *Magmatism in the Ocean Basins*. Geological Society of London Special Publications, 42: 313–345.

Taylor, S.R., and Mclennan, S.M., 1985. The continental crust: Its composition and evolution, an examination of the geochemical record preserved in sedimentary rocks. *Blackwell Sci. Publ. Oxford, UK*, 312.

Tao Yan, Gao Zhenmin, Luo Taiyi, Qi Jingdong, He Yingjun and Yang Tingxiang, 2002. Inversion of primary magma composition for Jinbaoshan ultramafic intrusion, Yunnan. *Acta Petrologica Sinica*, 18(1): 70–82 (in Chinese with English abstract).

Tao Yan, Gao Zhenmin, Luo Taiyi and Qi Jingdong, 2004. PGE in Jinbaoshan intrusion: Possible evidence of mantle plume origin. *Bulletin of Mineralogy, Petrology and Geochemistry*, 23(1): 28–31 (in Chinese with English abstract).

Tao Yan, Li Chusi, Hu Ruizhong, Ripley, E.M., Du Andao and Zhong Hong, 2007a. Petrogenesis of the Pt–Pd mineralized Jinbaoshan ultramaficintrusion in the Permian Emeishan Large Igneous Province, SW China. *Contrib. Mineral. Petrol*., 153: 321–337.

Tao Yan, Hu Ruizhong, Qi Liang and Luo Taiyi, 2007b. Geochemical characteristics and metallogenesis of the Limahe mafic-ultramafic intrusion, Sichuan. *Acta Petrologica Sinica*, 23(11): 2785–2800 (in Chinese with English abstract).

Tao Yan, Li Chusi, Song Xieyan and Ripley, E.M., 2008. Mineralogical, petrological, and geochemical studiesof the Limahe mafic–ultramatic intrusion and associated Ni–Cu sulfide ores, SW China. *Miner. Deposita.*, 43: 849–872.

Thompson, R.N., and Gibson, S.A., 2000. Transient high

temperatures in mantle plume heads inferred from magnesian olivines in Phanerozoic picrites. *Nature*, 407: 502–506.

Ulmer, P., 1989. The dependence of Fe^{2+}~Mg cation-partitioning between olivine and basaltic liquid on pressure, temperature and composition. Contrb. *Mineral. Petrol*., 101: 261–273.

Wang, C.Y., Zhou Meifu and Zhao Donggao, 2005. Mineral chemistry of chromite from the Permian Jinbaoshan Pt-Pd-sulphide-bearing ultramafic intrusion in SW China with petrogenetic implications. *Lithos*, 83: 47–66.

Wang, C.Y., Zhou Meifu and Keays, R.R., 2006. Geochemical constraints on the origin of the Permian Baimazhai mafic-ultramafic intrusion, SW China. Contrib. *Mineral. Petrol*., 152: 309–321.

Wang Denghong, Luo Yaonan, Fu Deming, Chu Yingshi and Lu Zhian, 2001. Petrochemistry and ore potentiality of the mafic-ultramafic rocks in the Yangliuping Cu-Ni-PGE mine, Sichuan Province. *Acta Geoscientia Sinica*, 22(2): 135–140 (in Chinese with English abstract).

Wang Yan, 2008. Origin of the Permian Baimazhai Magmatic Ni-Cu-(PGE) Sulfide Deposits, Yunnan: Implications for the Relationship of Crustal Contamination and Mineralization. *Bulletin of Mineralogy, Petrology and Geochemistry*, 27(4): 332–343 (in Chinese with English abstract).

Wu Fuyuan, Wilde, S.A., Zhang Guangliang and Sun Deyou, 2004. Geochronology and petrogenesis of the post-orogenic Cu, Ni sulfide-bearing mafic-ultramafic complexes in Jilin Province, NE China. *Journal of Asian Earth Sciences*, 23: 781–797.

Xiao Long, Xu Yigang, Mei Houjun, Zheng Yongfei, He Bin and Pirajno, F., 2004. Distinct mantle sources of low-Ti and high-Ti basalts from the western Emeishan large igneous province, SW China: Implications for plume-lithosphere interaction. *Earth and Planetary Science Letters*, 228: 525–546.

Xiong Shunhua and Li Jianlin, 1984. The characteristics of the late Permian basalts in the margin of continental rift in Emeishan area. *Journal of Chengdu College of Geology*, 30 (3): 43–59 (in Chinese with English abstract).

Xu Jifeng, Suzuki, K, Xu Yigang, Mei Houjun and Li Jie, 2007. Os, Pb and Nd isotope geochemistry of the Permian Emeishan continental flood basalts: Insights into the source of a large igneous province. *Geochimica et Cosmochimica Acta*, 71: 2104–2119.

Xu Yigang, Chung S.-L, John, B.M., and Wu Genyao, 2001. Petrologic and geochemical constraints on the petrogenesis of Permian–Triassic Emeishan flood basalts in southwestern China. *Lithos*, 58: 145–168.

Xu Yigang, He Bin, Chung Sunlin, Menzies, M.A., and Frey, F.A., 2004. Geologic, geochemical, and geophysical consequences of plume involvement in the Emeishan flood-basalt province. *Geology*, 32: 917–920.

Yao Jiadong, 1986. On the Genesis of Cu-(Pt)-Ni Sulfide Deposits in Xichang Region. *Chongqing: Chongqing Publishing House*, 34–37 (in Chinese with English abstract).

Zhang Zhaochong and Wang Fusheng, 2003. A method for identifying primary magma-Examples from picrite and alkali basalts. *Journal of Jilin University* (Earth Science Edition), 33 (2): 130–134 (in Chinese with English abstract).

Zhang Zhaochong, Mao Jingwen, Wang Fusheng, Hao Yanli and Mahoney, J.J., 2005a. Mantle plume activity and melting conditions: Evidences from olivines in picritic-komatiitic rocks from the Emeishan Large Igneous Province, southwestern China. *Episodes*, 28(3): 171–176.

Zhang Zhaochong, Wang Fusheng, Qu Wenjun, Hao Yanli and Mahomey, J.J., 2005b. Discovery of high-Os picrites in the large Emeishan Igneous Province and its geological significance. *Acta Geologica Sinica*, 79(4): 515–521 (in Chinese with English abstract).

Zhang Zhaochong, Mahoney, J.J., Mao Jingwen and Wang Fusheng, 2006. Geochemistry of picritic and associated basalt flows of the western Emeishan flood basalt province, China. *Journal of Petrology*, 47: 1997–2019.

Zhong Hong, Hu Ruizhong, Zhou Xinhua and Ye Zaojun, 2004. Geochemistry of the volcanic rocks in the Dapingzhang ore district, Simao, Yunnan province and its tectonic significance. *Acta Petrologica Sinica*, 20(3): 567–574 (in Chinese with English abstract).

Zhong Hong, Zhu Weiguang, Qi Liang, Zhou Meifu, Song Xieyan and Zhang Yi, 2006. Platinum group elements(PGE) geochemistry of Emeishan basalts in the Panxi area, SW China. *Chinese Science Bulletin* (English edition), 51(7): 845–854.

Zhou Meifu, Malpas, J., Song Xieyan, Robinson, P.T., Sun Min, Kennedy, A.K., Lesher, C.M., and Keays, R.R., 2002. A temporal link between the Emeishan large igneous province (SW China) and the end-Guadalu-pian mass extinction. *Earth and Planetary Science Letters*, 196(3–4): 113–122.

Zhou Meifu, Zhao Junhong, Qi Liang, Su Wenchao and Hu Ruizhong, 2006. Zircon U-Pb geochronology and elemental and Sr-Nd isotope geochemistry of Permian mafic rocks in the Funing area, SW China. *Contrib. Miner. Petrol*., 151: 1–19.

Zhou, M.F., Arndt, N.T., Malpas, J., Wang, C.Y., and Kennedy, A.K., 2008, Two magma series and associated ore deposit types in the Permian Emeishan Large Igneous Province, SW China. *Lithos*, 103, 352–368.

Zhu Dan, Xu Yigang, Luo Taiyi, Song Xieyan, Tao Yan, Huang Zhilong, Zhu Chengmin and Cai Enzhao, 2007. Conduit of the Emeishan basalts: The Zhubu mafic-ultramafic intrusion in the Yuanmou area of Yunnan Province, China. *Acta Mineralogica Sincia*, 27(3/4): 273–280 (in Chinese with English abstract).